Forced Secondary Circulations in Hurricanes

H. E. WILLOUGHBY

National Hurricane and Experimental Meteorology Laboratory, NOAA, Coral Gables, Florida 33124

In this study, application of Eliassen's (1951) forced secondary circulation model to the hurricane vortex is reexamined. It is shown by scale analysis that the symmetric tangential flow is in hydrostatic and gradient balance if the asymmetric part of the tangential flow and the radial and vertical symmetric motions are appreciably smaller than the symmetric tangential flow. When surface friction and cumulus transports of heat and momentum are included, the forced symmetric radial and vertical motions may be diagnosed. The approximations on which this system of balanced equations is based are valid everywhere in the hurricane vortex except in the upper tropospheric outflow layer. In the absence of Fickian diffusion of momentum and heat, both deep inflow in the outer vortex and subsidence within the eye are forced by radial gradients of convective heating. If corresponding gradients of cooling arise in the upper troposphere by mechanisms such as detrainment from overshooting cumuli, descent may be induced in the lower stratosphere above and around the eye. Convective momentum transports act to weaken the thermally induced secondary flow somewhat. If the vertical resolution of the finite difference mesh is too coarse to resolve the detrainment layer properly, the model may diagnose an unrealistic secondary flow with ascent throughout the eye. In the absence of all cumulus processes, the frictionally converged air no longer rises to the tropopause but rather flows outward in a shallow layer in the lower troposphere.

INTRODUCTION

In the balanced formulation of hurricane models, the tangential flow is assumed to be in gradient balance and hydrostatic equilibrium, and the radial and vertical motions are diagnosed with a technique developed by *Eliassen* [1951]. *Estoque* [1962] and *Rosenthal* [1963] attempted to obtain the secondary flows induced in hurricanes by explicit large-scale condensational heating with this method. Both models exhibited shallow frictional inflow near the surface and outflow which was concentrated below the midtroposphere, with the strongest radial velocities just above the friction layer. *Ogura* [1964], following the lead of *Charney and Eliassen* [1964], formulated a balanced model in which the condensational heating aloft was proportional to the convergence of water vapor in the frictional boundary layer. His solutions resembled real hurricanes but did not go to a steady state analogous to the mature storm. Subsequent models of *Kuo* [1965], *Ooyama* [1969], and *Sundqvist* [1970*a*, *b*] were also formulated on the same basis. Although the first two of these had limited vertical resolution, Sundqvist's model had 10 levels in the vertical and produced a realistic secondary circulation with descent inside the eye, a shallow upper tropospheric outflow layer, and deep inflow in the lower troposphere. In addition to the balanced models, symmetric, primitive equation models [e.g., *Yamasaki*, 1968*a*, *b*; *Rosenthal*, 1970*a*, *b*; *Anthes*, 1971] as well as three- dimensional, primitive equation models [*Anthes et al.*, 1971; *Kurihara and Tuleya*, 1974; *Mathur*, 1974; *Jones*, 1977] have dominated the field. However, recently, *Peng and Kuo* [1975] introduced a hybrid 10-level symmetric model with a primitive equation boundary layer and a balanced free atmosphere. The cumulus parameterization acted to vertically redistribute latent heat converged in the boundary layer, and they attempted to include convective momentum transports by increasing the vertical momentum diffusivity in regions of strong boundary layer convergence.

The present work is primarily a physical interpretation of the diagnostic portion of a conventional balanced model. The balanced governing equations, as well as a set of linear nonbalanced equations that describe the asymmetric motions, are established by scale analysis of the primitive equations. These scaling arguments are related to those of *Ogura* [1964] and, to a lesser extent, to those of *Anthes* [1974]. The balanced equations are shown to be valid when the radial, vertical, and asymmetric motions are small in comparison to the symmetric tangential flow.

The convective heating and momentum transports are parameterized with a 'second-generation' scheme [*Ooyama* 1971; *Fraedrich*, 1973; *Arakawa and Schubert*, 1974; *Schneider and Lindzen*, 1976], and the secondary circulation is diagnosed with the balanced equations. This model has no explicit diffusion of either heat or momentum; the only forcing agents are the convective processes and surface friction. The results obtained allow novel interpretations of several features of hurricane dynamics.

Recent work by *Yamasaki* [1977*a*, *b*] and *Rosenthal* [1978, 1979] indicates that explicit calculation of convective effects may be preferable to parameterized schemes in full scale numerical models. Although it does seem that the future of hurricane modeling lies in this direction, it is still possible to obtain useful insight with the present formulation.

SCALE ANALYSIS

Consider the primitive equations expressed in cylindrical, log pressure coordinates centered on the vortex and moving with it. At the outset the anelastic approximation [*Ogura and Phillips*, 1962] is made to eliminate acoustic waves. Coriolis forces arising from the storm's motion, environmental pressure gradients, friction, and convective transports are included in the forcing terms on the right sides:

$$\frac{\partial u}{\partial t} + \frac{v}{r}\frac{\partial u}{\partial \lambda} + u\frac{\partial u}{\partial r} - v\left(\frac{v}{r} + f\right) + w\frac{\partial u}{\partial z} + \frac{\partial \phi}{\partial r} = \mathrm{U} \quad (1a)$$

$$\frac{\partial v}{\partial t} + \frac{v}{r}\frac{\partial v}{\partial \lambda} + u\left(\frac{\partial v}{\partial r} + \frac{v}{r} + f\right) + w\frac{\partial v}{\partial z} + \frac{1}{r}\frac{\partial \phi}{\partial \lambda} = \mathrm{V} \quad (1b)$$

$$\frac{\partial w}{\partial t} + \frac{v}{r}\frac{\partial w}{\partial \lambda} + u\frac{\partial w}{\partial r} + w\frac{\partial w}{\partial z} - b + \frac{\partial \phi}{\partial z} = \mathrm{W} \quad (1c)$$

$$\frac{\partial b}{\partial t} + \frac{v}{r}\frac{\partial b}{\partial \lambda} + u\frac{\partial b}{\partial r} + N^2 w = \mathrm{B} \quad (1d)$$

Paper number 9C0098.

$$\frac{\partial u}{\partial r} + \frac{u}{r} + \frac{1}{r}\frac{\partial v}{\partial \lambda} + \frac{\partial w}{\partial z} - \frac{w}{H} = 0 \qquad (1e)$$

The variables used are

- r radius;
- z vertical coordinate;
- λ azimuth;
- t time;
- u radial wind component;
- v tangential wind component;
- w vertical wind component;
- b buoyancy, equal to $g(T - T_r)/T_r$;
- ϕ geopotential;
- N^2 square of the buoyancy frequency, equal to $g(\gamma_d - \gamma)/T_r$];
- f Coriolis frequency;
- H scale height;
- T temperature;
- T_r reference temperature in the undisturbed atmosphere;
- γ lapse rate;
- γ_d dry adiabatic lapse rate;
- g gravitational acceleration;
- U, V, W, B forcing of the corresponding dependent variables.

The system in (1) is nondimensionalized with the following scales:

$$\begin{aligned} v &= Vv^* & V &\sim 50\ \text{m s}^{-1} \\ u &= Uu^* & U &\sim 10\ \text{m s}^{-1} \\ w &= Ww^* & W &\sim 10\ \text{m s}^{-1} \\ b &= Bb^* & B &\sim UV/Z \\ r &= Rr^* & R &\sim 15\ \text{km} \\ z &= Zz^* & Z &\sim 15\ \text{km} \\ \phi &= \mu g H \phi^* & \mu &\sim 0.05 \\ t &= (R/V)t^* & & \\ H &= Zh^*/2 & & \end{aligned} \qquad (2)$$

where the asterisk denotes nondimensional variables. This scaling is appropriate to the eye wall regions. Below, it is extended to the outer portions of the storm to obtain a set of equations that describe motions throughout the lower troposphere.

The continuity equation (1e) is treated first:

$$\frac{U}{R}\left(\frac{\partial u^*}{\partial r^*} + \frac{u^*}{r^*}\right) + \frac{V}{R}\left(\frac{1}{r^*}\frac{\partial v^*}{\partial \lambda}\right) + \frac{W}{Z}\left(\frac{\partial w^*}{\partial z^*} - \frac{2w^*}{h^*}\right) = 0 \qquad (3)$$

If the dependent variables may be represented in terms of an asymptotic expansion in $\epsilon \sim U/V$,

$$\begin{aligned} u^* &= u_0 + \epsilon u_1 + \epsilon^2(\cdots \\ v^* &= v_0 + \epsilon v_1 + \epsilon^2(\cdots \\ w^* &= w_0 + \epsilon w_1 + \epsilon^2(\cdots \\ b^* &= b_0 + \epsilon b_1 + \epsilon^2(\cdots \\ \phi^* &= \phi_0 + \epsilon \phi_1 + \epsilon^2(\cdots \end{aligned} \qquad (4)$$

Substitution into (3) and collection of like powers ϵ give

$$\begin{aligned} &\frac{\partial u_0}{\partial r^*} + \frac{u_0}{r^*} + \frac{1}{r^*}\frac{\partial v_1}{\partial \lambda} + \frac{\partial w_0}{\partial z^*} - \frac{2w_0}{h^*} = 0 \\ &\frac{\partial v_0}{\partial \lambda} = 0 \end{aligned} \qquad (5)$$

since $U \sim W \sim \epsilon V$. Thus at zero order, tangential wind is axisymmetric, and the asymmetries have the same scale as the radial and vertical motions. One expects that the tangential wind will be in something like gradient balance, so the buoyancy and geopotential should have zero-order symmetric and first-order asymmetric parts as well.

If one were to substitute directly from (2) into the tangential momentum (1b) and buoyancy (1d) equations, the only terms present at zero order would be $\partial v_0/\partial t^*$ and $\partial b_0/\partial t^*$. However, introduction of a slow time scale for the symmetric motions transforms these terms to first order. One thus chooses $\epsilon^{-1}t^*$ to represent the gradual evolution of the symmetric vortex under radial and vertical advection. Henceforth the subscripts s and a indicate the symmetric and asymmetric parts of the variable in question. Thus the zero-order parts of u^* and w^* are rewritten as $u_a + u_s$ and $w_a + w_s$; v_0, b_0, and ϕ_0 are redesignated v_s, b_s, and ϕ_s; and v_1, b_1, and ϕ_1 are redesignated v_a, b_a, and ϕ_a. In this notation, (4) becomes

$$\begin{aligned} u^* &= u_s(r^*, z^*, \epsilon^{-1}t^*) + u_a(r^*, z^*, \lambda, t^*) + \epsilon(\cdots \\ v^* &= v_s(r^*, z^*, \epsilon^{-1}t^*) + \epsilon v_a(r^*, z^*, \lambda, t^*) + \epsilon^2(\cdots \\ w^* &= w_s(r^*, z^*, \epsilon^{-1}t^*) + w_a(r^*, z^*, \lambda, t^*) + \epsilon(\cdots \\ b^* &= b_s(r^*, z^*, \epsilon^{-1}t^*) + \epsilon b_a(r^*, z^*, \lambda, t^*) + \epsilon^2(\cdots \\ \phi^* &= \phi_s(r^*, z^*, \epsilon^{-1}t^*) + \epsilon \phi_a(r^*, z^*, \lambda, t^*) + \epsilon^2(\cdots \end{aligned} \qquad (6)$$

The remaining relations (1a–1d) are now nondimensionalized with (2), substitution from (6) is made, and both the symmetric and asymmetric components of the forcing are chosen to be order 1 in ϵ. Collection of like powers of ϵ yields the following at zero order:

$$\begin{aligned} &\frac{v_s^2}{r^*} + \frac{v_s}{R^*} = \frac{\mu}{F^*}\frac{\partial \phi_s}{\partial r^*} \\ &b_s = \frac{\mu}{F^*}\frac{\partial \phi_s}{\partial z^*} \\ &\frac{\partial u_s}{\partial r^*} + \frac{u_s}{r^*} + \frac{\partial w_s}{\partial z^*} - \frac{2w_s}{h^*} = 0 \end{aligned} \qquad (7)$$

and at first order,

$$\begin{aligned} &\frac{\partial u_a}{\partial t^*} + \frac{v_s}{r^*}\frac{\partial u_a}{\partial \lambda} - \xi^* v_a + \frac{\mu}{F^*}\frac{\partial \phi_a}{\partial r^*} = \mathsf{U}_s^* + \mathsf{U}_a^* \\ &\frac{\partial v_s}{\partial t^*} + \frac{\partial v_a}{\partial t^*} + \frac{v_s}{r^*}\frac{\partial v_a}{\partial \lambda} + (u_s + u_a)\xi^* + (w_s + w_a)S^* \\ &\qquad + \frac{\mu}{F^*}\frac{1}{r^*}\frac{\partial \phi_a}{\partial \lambda} = \mathsf{V}_s^* + \mathsf{V}_a^* \\ &A^{*2}\left(\frac{\partial w_a}{\partial t^*} + \frac{v_s}{r^*}\frac{\partial w_a}{\partial \lambda}\right) - b_a + \frac{\mu}{F^*}\frac{\partial \phi_a}{\partial z^*} = A^*(\mathsf{W}_s^* + \mathsf{W}_a^*) \\ &\frac{\partial b_s}{\partial t^*} + \frac{\partial b_a}{\partial t^*} + \frac{v_s}{r^*}\frac{\partial b_a}{\partial \lambda} + (u_s + u_a)\frac{\partial b_s}{\partial r^*} \\ &\qquad + R_i^* N^{*2}(w_s + w_a) = \mathsf{B}_s^* + \mathsf{B}_a^* \\ &\frac{\partial u_a}{\partial r^*} + \frac{u_a}{r^*} + \frac{1}{r^*}\frac{\partial v_a}{\partial \lambda} + \frac{\partial w_a}{\partial z^*} - \frac{2w_a}{h^*} = 0 \end{aligned} \qquad (8)$$

where $F^* = gH/V^2$, $R_i^* = Z^2N^2/V^2$, and $R^* = V/fR$ are the Froude, Richardson, and Rossby numbers, respectively. $N^{*2}(r^*, z^*)$ and $h^*(r^*, z^*)$ are of order unity; their variations account for spatial changes in the symmetric temperature field

over the domain. In the vortex core the aspect ratio and μ divided by the Froude number are of order unity, the Rossby number is about 10^{-2}, and the Richardson number is 9 for $V \sim 50$ m s^{-1}. Strictly speaking, terms in R^{*-1} could be omitted, but it is shown below that their retention greatly increases the generality of the equations. Following the notation of *Willoughby* [1977], $\zeta^* = (\partial v_s/\partial r^* + v_s/r^* + 1/R^*)$, $\xi^* = 2v_s/r^* + 1/R^*$, and $S^* = \partial v_s/\partial z^*$ are the vorticity, inertia parameter, and vertical shear of the symmetric tangential motion, respectively.

The symmetric and asymmetric motions are separated by azimuthally averaging (8). U_s^* and W_s^* are seen to be zero. Replacement of μ/F^* and A^* with the unity and combination of the averaged equations with (7) form the complete set of balanced equations for the symmetric motions:

$$\frac{v_s^2}{r^*} + \frac{v_s}{R^*} = \frac{\partial \phi_s}{\partial r^*} \tag{9a}$$

$$\frac{\partial v_s}{\partial t^*} + u_s\zeta^* + w_s S^* = V_s^* \tag{9b}$$

$$b_s = \frac{\partial \phi_s}{\partial z^*} \tag{9c}$$

$$\frac{\partial b_s}{\partial t^*} + u_s\frac{\partial b_s}{\partial r^*} + R_i^* N^{*2} w_s = B_s^* \tag{9d}$$

$$\frac{\partial u_s}{\partial r^*} + \frac{u_s}{r^*} + \frac{\partial w_s}{\partial z^*} + \frac{2w_s}{h^*} = 0 \tag{9e}$$

Subtraction of (9*b*) and (9*d*) from the corresponding relations in (8) gives a set that describes the asymmetric motions:

$$\frac{\partial u_a}{\partial t^*} + \frac{v_s}{r^*}\frac{\partial u_a}{\partial \lambda} - \xi^* v_a + \frac{\partial \phi_a}{\partial r^*} = U_a^*$$

$$\frac{\partial v_a}{\partial t^*} + \frac{v_s}{r^*}\frac{\partial v_a}{\partial \lambda} + \zeta^* u_a + S^* w_a + \frac{1}{r}\frac{\partial \phi_a}{\partial \lambda} = V_a^*$$

$$\frac{\partial w_a}{\partial t^*} + \frac{v_s}{r^*}\frac{\partial w_a}{\partial \lambda} - b_a + \frac{\partial \phi_a}{\partial z} = W_a^* \tag{10}$$

$$\frac{\partial b_a}{\partial t^*} + \frac{v_s}{r^*}\frac{\partial b_a}{\partial \lambda} + \frac{\partial b_s}{\partial r^*}u_a + R_i^* N^{*2} w_a = B_a^*$$

$$\frac{\partial u_a}{\partial r^*} + \frac{u_a}{r^*} + \frac{1}{r^*}\frac{\partial v_a}{\partial \lambda} + \frac{\partial w_a}{\partial z^*} - \frac{2w_a}{h^*} = 0$$

The solutions of (10) have been explored in some detail by *Willoughby* [1977, 1978*a*, *b*].

Consider a second scaling appropriate to the outer portion of the domain where the Rossby number is about 1. Here, some of the scaling parameters assume new values:

$$\begin{aligned} V &\sim 10 \text{ m s}^{-1} \\ U &\sim 3 \text{ m s}^{-1} \\ R &\sim 300 \text{ km} \\ \mu &\sim 10^{-3} \\ R^* &\sim \mu/F^* \sim 1 \\ A^* &\sim 5 \times 10^{-2} \end{aligned} \tag{11}$$

and the remainder are unchanged from their previous values. Substitution into (1*a*)–(1*e*) and manipulation similar to that just described lead to equations closely resembling (9*a*)–(9*e*) and (10). The new equations differ from the old only in that the asymmetric motions are hydrostatic and the Rossby number is everywhere replaced by 1. Thus (9) and (10) correctly describe the motions everywhere in the domain, even though the variables might seem to get out of scale ($r^* \sim 10$, $v_s \sim 0.1$, etc.) as one moves out from the center. In summary, the only restrictions on the validity of these equations are that the evolution of the symmetric motions must be appreciably slower than the time required for tangential advection to change the fields significantly, the momentum forcing must lead to accelerations much smaller than the centrifugal acceleration, and the ratio of the asymmetric, radial, and vertical velocities to the symmetric tangential velocity must be small. These conditions are easily met in the lower troposphere, but the flow is strongly asymmetric, and the tangent of the crossing angle exceeds 1 in the outflow layer. Philosophically, presentation of solutions in the latter region is justified only by their resemblance to the results of primitive equation models and to hurricanes in nature.

An alternative scaling arises in case the tangential momentum or buoyancy forcing is of order zero in ϵ. This leads to a balance between $\partial v_s/\partial t^*$ and $\partial b_s/\partial t^*$ and the forcing, thus precluding introduction of the slow time scale for the strongly forced variables. The motions that arise in this scaling are unlike those in a hurricane, so the decisions to introduce the slow time scale and to require U_s^* and B_s^* to be of order 1 are justified a posteriori.

Analysis based upon decomposition of the variables into symmetric and asymmetric components has led to significant advances in the study of the large-scale atmosphere [e.g., *Holton*, 1975]. The present analysis is analogous to that approach and represents essentially a small-amplitude linearization about the mean vortex, although it does not offer the same degree of accuracy as in the large-scale case.

OBSERVATIONS

In this section some observational justification for the preceding scaling argument is presented. During the night of September 1–2, 1977, one of the WP3-D aircraft of NOAA's Research Facilities Center operated at 700 mbar in hurricane Anita [*Sheets*, 1977]. This was the first such flight in which a new data acquisition system was fully operational, and data of unprecedented quality were obtained. Here, analysis of a subset of these data is presented. The subset was obtained between 0028 and 0513 UT on September 2 and consists of four radial profiles along each cardinal compass direction from the center, for a total of 16 profiles. The data were originally collected at 1-s intervals (about every 100 m along the aircraft track) and are presented as 2-km running averages evaluated every 0.5 km.

The profiles along a line extending south from the center are typical of the other observations and are shown in Figure 1*a*. The dashed and solid curves represent an outward pass and the subsequent inward flight. Each leg required 20 min of flying time to complete, so the maximum interval between observations at the same point is only 40 min in this pair. Then about 2 hours elapsed between completion of the dashed leg and the beginning of the dotted and chain-dashed legs. These last two are also successive passes completed within a 40-min period.

All of the winds are derived from the aircraft inertial navigation equipment. In the case of the radial and vertical velocities there seems to be little correlation between radial legs, but the tangential velocity shows radial structure that persists from profile to profile. This is also true of the 700-mbar height and the temperature. This is emphasized in Figure 1*b*, which represents an approximation to the azimuthal mean obtained by averaging all 16 radial profiles. The ring of rising motion just inside the radius of maximum wind is the only feature of the

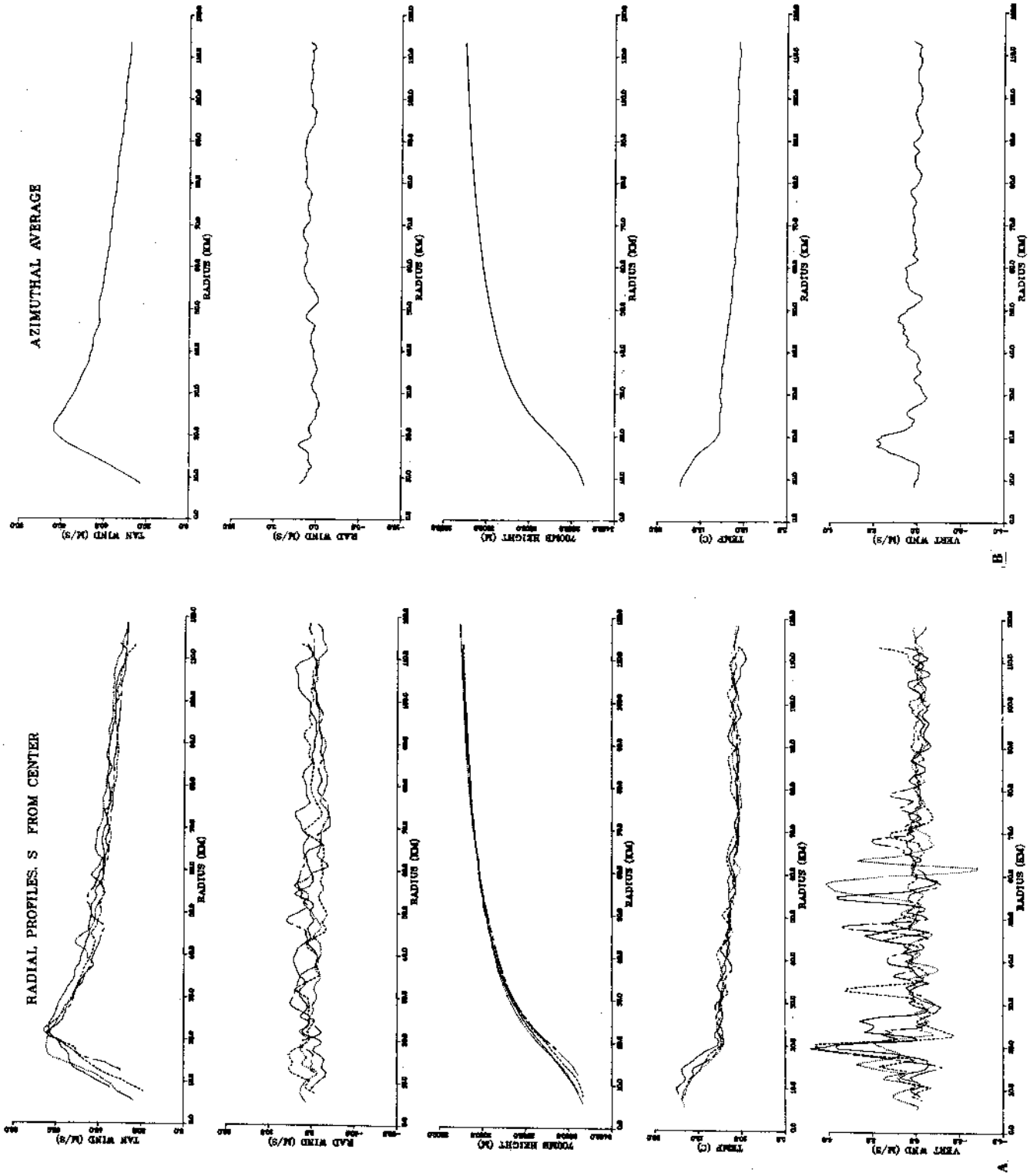
AZIMUTHAL AVERAGE
RADIAL PROFILES, S FROM CENTER
TAN WIND (M/S)
RAD WIND (M/S)
700MB HEIGHT (M)
TEMP (C)
VERT WND (M/S)
RADIUS (KM)
A
B

variables with fast zero-order parts in (6) to survive the averaging. This, of course, corresponds to w_s. On the other hand, the symmetric structure of the variables without zero-order asymmetries dominates their radial variation. If the azimuthal mean were subtracted from the curves in Figure 1*a*, the radial variations of the residuals would resemble those of the fast zero-order variables and would have an amplitude consistent with the scaling in the previous section. It is observations such as these that inspired the choice of magnitudes and time scales for the fast and slow variables.

Equation (9*a*) predicts that the gradient wind relation should be valid in the azimuthal average below the outflow layer. Figure 2*a* shows, as a function of radius, the azimuthal average tangential wind from Figure 1*b* in comparison to the gradient wind computed from the symmetric geopotential. In calculating that quantity the 700-mbar height was numerically differentiated, a three-point smoother was applied 10 times, and then the gradient wind formula was entered. Figure 2*b* is a scatter diagram relating the gradient and observed tangential wind. The observed and gradient winds generally lie within 10% of each other. This agreement is actually somewhat better than the scaling would indicate and is supported by earlier work by *Hawkins and Rubsam* [1968].

Gray and Shea [1973], in their study of a composite hurricane based on aircraft data, contradict these results. They report centripetal accelerations near the radius of maximum wind (RMW) that exceed the gradient value by 20–50%. These large supergradient values seem unreasonable. If the v_s^2/r^* term were 110% of the pressure gradient acceleration and were to prevail over a 5-km interval just inside the RMW in a hurricane with a 15-km radius eye and a 50-m s^{-1} maximum wind speed, the outward radial velocity induced at the outer end of the interval would be nearly 13 m s^{-1} if the initial value were zero. Gray and Shea's composite hurricane shows outflow equal to 5 m s^{-1} at 5 km inside the RMW and decreasing to zero at the RMW; the decrease takes place over the interval where the strongest supergradient winds lie.

It may be that the excessive supergradient values are an artifact of the way in which the composites were taken. In the process of compositing, the radial profiles along many different azimuths in several storms were adjusted so that their RMW's corresponded, and the averages were computed on the basis of distance from the RMW rather than distance from the center. Suppose that the tangential wind in each profile is the sum of a symmetric flow that is in gradient balance and a radially varying asymmetric motion that is not. The sum will usually be supergradient near the maxima of the asymmetric component and subgradient near its minima. In each profile the apparent RMW for the sum will tend to occur at the radial maximum of the asymmetric motion nearest the symmetric maximum. Thus after the profiles are averaged with respect to the RMW the winds at the apparent RMW will seem to be supergradient, although the azimuthal average tangential wind at the average RMW is nearly balanced.

The balanced equations show that the momentum forcing in the tangential direction induces radial motion that advects angular momentum of the appropriate sign to restore gradient balance. The azimuthally averaged tangential flow can differ appreciably from the gradient value only when the radial acceleration is large.

MODEL

The symmetric, balanced governing equations (9*a*)–(9*e*) form the basis of the time-dependent balanced models cited in the introduction. The present model uses the same equations to diagnose the forced radial and vertical motions and does not attempt to treat the evolution of the vortex. The structure of the buoyancy, geopotential, tangential velocity, and heating rate are specified to resemble an intense, mature hurricane that is continuing to intensify, so the solutions are an instantaneous representation of the secondary flow at that stage in the storm's evolution.

The balanced governing equations are manipulated following *Eliassen* [1951] to obtain a single partial differential equation for θ, the stream function in the r^*-z^* plane:

$$\left(\frac{\partial}{\partial r^*}-\frac{1}{r^*}\right)\left(R_i^* N^{*2}\frac{\partial \psi}{\partial r^*}-S^*\xi^*\frac{\partial \psi}{\partial z^*}\right)+\left(\frac{\partial}{\partial z^*}+\frac{2}{h^*}\right)\left(\zeta^*\xi^*\frac{\partial \psi}{\partial z^*}-S^*\xi^*\frac{\partial \psi}{\partial r^*}\right)=-\left(\frac{\partial}{\partial z^*}+\frac{2}{h^*}\right)(\xi^* r^*\rho^* V_s^*)+\left(\frac{\partial}{\partial r^*}-\frac{1}{r^*}\right)(r^*\rho^* B_s^*) \tag{12}$$

where $u_s = -(1/r^*\rho^*)(\partial\psi/\partial z^*)$ and $w_s = (1/r^*\rho^*)(\partial\psi/\partial r^*)$.

Qualitative discussion of the solutions to (12) is available in Eliassen's original paper and in *Holton*'s [1972] text. Briefly, (12) is a Poisson equation. Regions of forcing of a particular sign tend to be occupied by stream function gyres of the opposite sign. For the present case the forcing is usually dominated by the horizontal derivative of the heating and the vertical derivative of the momentum convergence. Thus when the former is increasing radially or when the latter is decreasing upward, a negative (out at low levels and inward aloft) gyre forms. Either an outward decrease in heating or an upward increase in momentum forcing induces a positive gyre. This equation describes the relation of thermodynamic and momentum forcing with both components of the secondary flow. If one attempts to diagnose the flow from the buoyancy (9*d*) or momentum equation (9*b*) alone, he may be seriously misled because he has neglected the way the motions are coupled through mass continuity.

Equation (12) is solved by the method of *Lindzen and Kuo* [1969], subject to the appropriate boundary conditions. The finite difference grid used is square, with intervals of 0.1 nondimensional unit, or about 1.5 km. The vertical resolution is comparable to that used in the 10-level models cited, but the horizontal resolution is much finer than the 20–30 km generally used in such work. Furthermore, the domain in the present model extends to $z^* = 2.0$, or about 15 km above the tropopause. This is much deeper than the domains used in previous work.

The surface boundary condition is the same as that used by *Ogura* [1964]. The stress at the surface is given by a quadratic stress law with drag coefficient $C_D = 3 \times 10^{-3}$ and is assumed to decrease to zero between the surface and the first interior information level. Integration of the tangential momentum equation (9*b*) from $z^* = 0$ to $z^* = \delta z^*$ gives an expression for the total radial mass flux in the boundary layer:

$$\psi(r^*, \delta z^*) = -\int_0^{\delta z^*} \rho^* r^* u_s \, dz^* \simeq C_D v_s^2 \rho^*(0)\, r^*/\zeta^* \tag{13}$$

Fig. 1. (Opposite) (*a*) Radial profiles of tangential and radial wind, 700-mbar height, temperature, and vertical velocity observed by aircraft on September 2, 1977, along a line extending south from the center of Hurricane Anita. (*b*) Azimuthal averages of the same quantities.

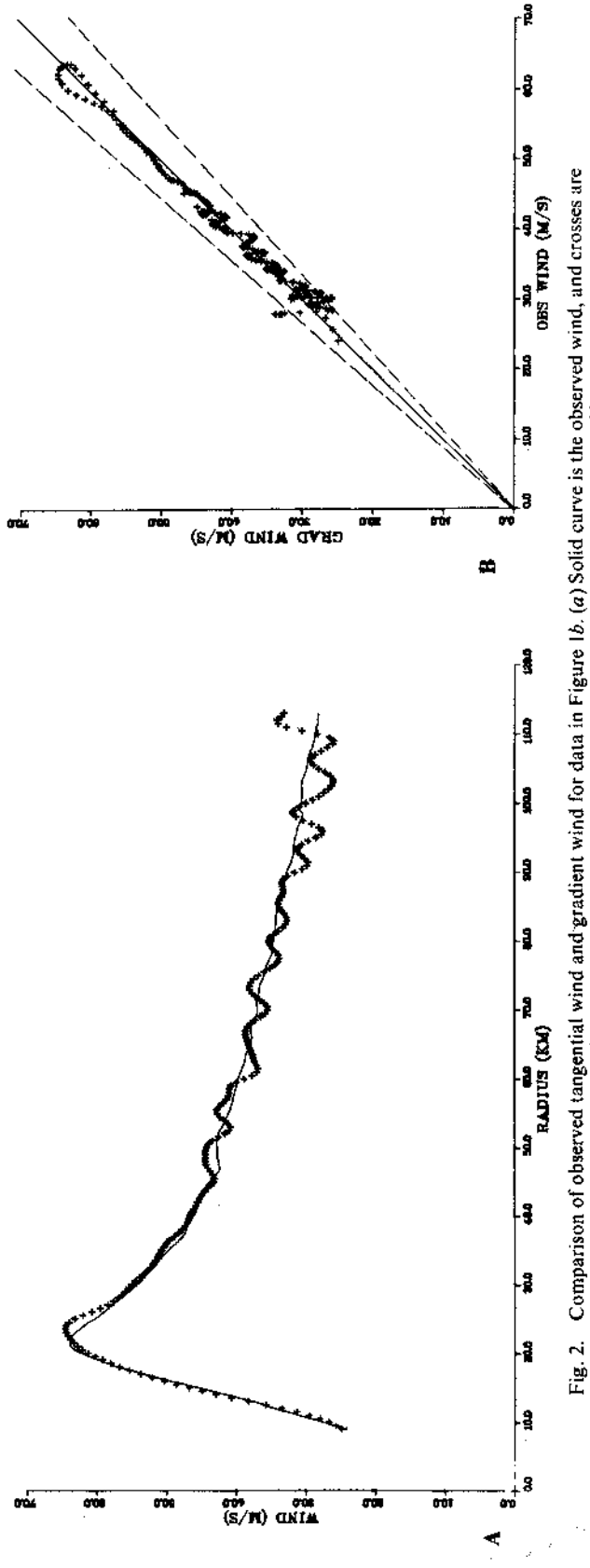

Fig. 2. Comparison of observed tangential wind and gradient wind for data in Figure 1*b*. (*a*) Solid curve is the observed wind, and crosses are the gradient wind. (*b*) Scatter diagram relating these quantities. Dashed lines represent ±10% error.

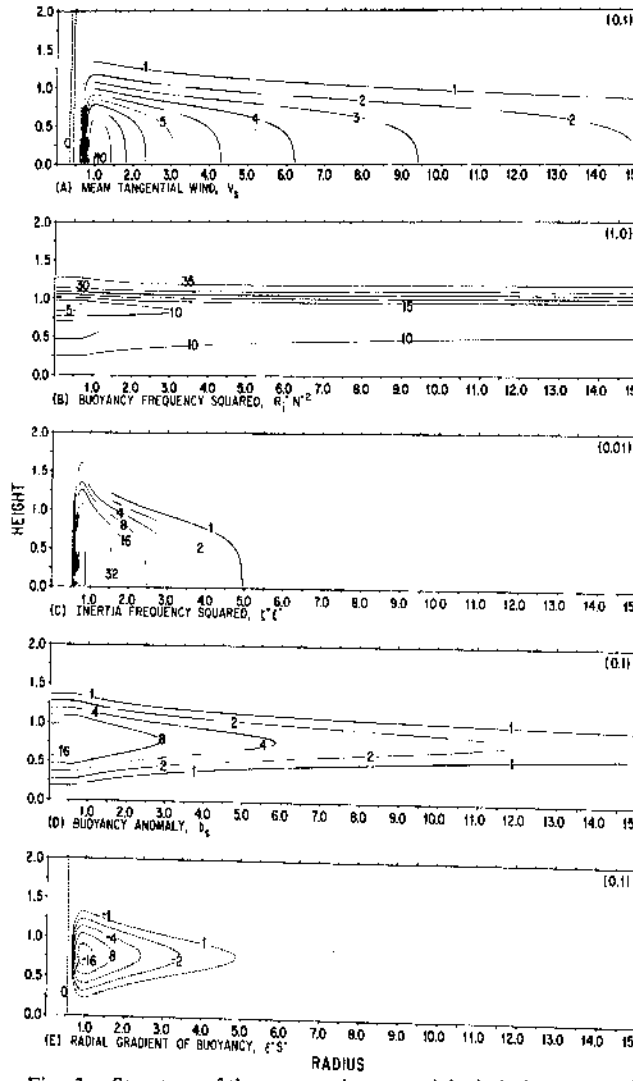

Fig. 3. Structure of the symmetric tangential wind, the symmetric buoyancy, and the coefficients in the differential equation for ψ. The tropopause is at $z^* = 1.0$, and the radius of maximum wind is at $r^* = 1.0$. The number in the upper right-hand corner in each panel indicates the nondimensional value that corresponds to a contour value of 1.0.

where $\psi(r^*, 0) = 0$ and $\partial v_s/\partial t^*$ and $\partial v_s/\partial z^*$ have been neglected in the boundary layer. The value of $\psi(r^*, \delta z^*)$ thus obtained is then used as a lower boundary condition in the numerical solution for ψ at the other interior points. In addition, $\partial\psi/\partial r^*|_{\delta z^*}$ is used to supply the vertical cloud base mass flux for the cumulus parameterization.

The other boundary conditions on ψ are $\psi(0, z^*) = \psi(r^*, 2) = 0$ and $\partial\psi/\partial r|_{r^*=50} = 0$. The center boundary condition is rigorously justified on the basis of axisymmetry, while the top and outer boundaries are so remote from the part of the domain in which we are interested that the solutions are insensitive to them.

The structure of the tangential flow, the buoyancy anomaly that supports it, and the principal coefficients in (12) are illustrated in Figure 3. These fields were designed to reflect hydrostatic and gradient balance, to resemble the observed structure of hurricanes reported by *Shea and Gray* [1973] and *Gray and Shea* [1973], and to avoid hydrodynamic instability.

The forcing arises from surface friction or from cumulus transport of buoyancy or momentum. The cumulus processes are parameterized with a scheme related to that of *Hayes*

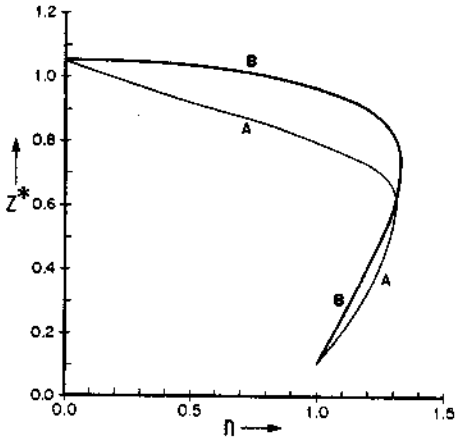

Fig. 4. Vertical variations of the two normalized cumulus mass flux profiles used in this study.

[1977] with the addition of momentum transports after *Schneider and Lindzen* [1976]. The scheme employs a model of a single cloud that extends from the surface to the tropopause and may entrain or detrain at any level. M_c, the total vertical mass flux carried by the clouds in an annular ring at radius r^*, is

$$M_c = \eta(z^*)\left.\frac{\partial \psi}{\partial r^*}\right|_{\delta z^*} \qquad \left.\frac{\partial \psi}{\partial r^*}\right|_{\delta z^*} > 0$$
$$M_c = 0 \qquad \left.\frac{\partial \psi}{\partial r^*}\right|_{\delta z^*} \leq 0 \tag{14}$$

where

$$\frac{1}{\eta}\frac{\partial \eta}{\partial z^*} = [\epsilon - \delta(z^*)] \tag{15}$$

Here ϵ and δ are fractional rates of entrainment and detrainment as functions of height. Figure 4 shows the two profiles of η used in this study. In both cases, ϵ is fixed at 1.0—equivalent to a vertical increase in η by a factor of e between the surface and the tropopause in the absence of detrainment. The detrainment rate is zero in the lower troposphere and increases to a large value near the tropopause. At the level where the entrainment and detrainment rates are equal, the mass flux attains a maximum, and it decreases to zero just above the tropopause. It is differences in the vertical variations in $\delta(z^*)$ that lead to the differences between the mass flux profiles. Both were chosen to resemble those diagnosed in observational studies of tropical waves [*Yanai et al.*, 1973; *Ogura and Cho*, 1973] and in the outer parts of tropical cyclones [*Frank*, 1977*b*], but neither profile includes the effect of shallow cumuli. Profile A has a fairly deep detrainment layer, but detrainment in B takes place in such a shallow interval that

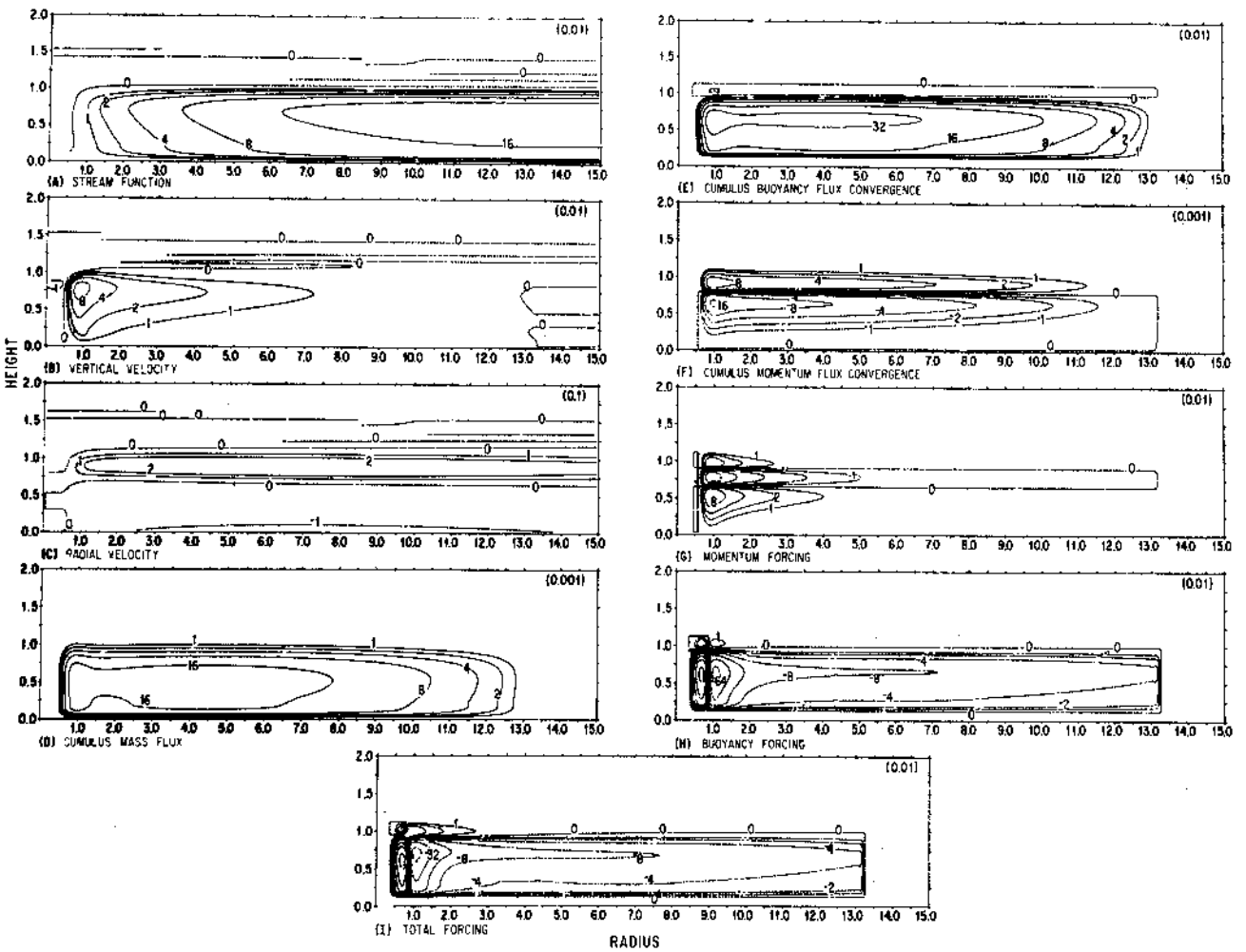

Fig. 5. Secondary circulation and its forcing for mass flux profile A. This simulation includes convective momentum transports. With the exception of the velocity components all quantities that appear in this figure are weighted with density and radius.

it is poorly resolved by the model. The former profile leads to a fairly realistic secondary flow, but the latter is used to illustrate some of the difficulties inherent in cumulus parameterization.

The apparent convective buoyancy and momentum sources [*Ogura and Cho*, 1973; *Schneider and Lindzen*, 1976] are given by

$$B_s^* = \frac{g^* M_c}{T_s}\left[\left(\frac{\partial T_s}{\partial z^*} + \gamma_d^*\right) + \delta(T_c - T_s)\right] \quad (16)$$

$$V_s^* = M_c[S^* + \delta(v_c - v_s)] \quad (17)$$

where g^* and γ_d^* are the nondimensional equivalents of g and γ_d as previously defined. Temperatures are nondimensionalized with 300°K, T_s is the nondimensional temperature corresponding to b_s, and T_c and v_c are the temperature and tangential velocity inside the clouds. Form drag on the clouds and the effects of evaporation or detrained water are neglected. The vertical variations of the in-cloud quantities are given by

$$\frac{\partial v_c}{\partial z^*} = -\epsilon(v_c - v_s) \quad (18a)$$

$$\frac{\partial h_c}{\partial z^*} = -\epsilon(h_c - h_s) \quad (18b)$$

$$T_c - T_s = (h_c - h_s)/[C_p + (L^2 q_s/R_v T_s^2)] \quad (18c)$$

where q_s is the mixing ratio in the unsaturated symmetric cloud environment and h_c and h_s are the moist static energies ($C_pT + Lq + g^*z^*$) of the clouds and environment, respectively. L is the latent heat of condensation, R_v is the gas constant for water vapor, and C_p is the specific heat at constant pressure for dry air. The last of these relations (equation (18*c*)) is used only to describe detrainment, and it requires that latent and sensible heat be detrained in such a ratio that the relative humidity remains constant. This is somewhat arbitrary, but at the levels where significant detrainment occurs, the temperature is so low that the air can hold little moisture. Thus the convective heating or cooling is insensitive to this assumption.

The cumulus parameterization is oversimplified in comparison to spectral schemes such as those proposed by *Ooyama* [1971] or *Arakawa and Schubert* [1974] and neglects such important effects as cumulus downdrafts [*Johnson*, 1976]. The problem is closed by initial specification of η and by requiring all of the boundary layer convergence to feed the cloud base mass flux. The vertical structure of the normalized mass flux does not respond to variations in stability. The parameterization may thus overestimate the amount of both deep convection and overshooting near the vortex center. In addition to cooling by detrainment from overshooting cumuli the cirrus canopy should cool radiatively, so the actual amount of upper tropospheric cooling is uncertain.

This parameterization is by no means unique. It was designed by trial and error to produce a realistic secondary circulation. In the next section it will be shown that the results are sensitive to the details of the parameterization. This suggests that such schemes may not provide a basis for successful time-dependent models of hurricanes. Nevertheless, this scheme is adequate for the more tractable problem of the vortex's response to realistic heat and momentum transports.

RESULTS

Figure 5 shows a forced secondary circulation and the convective forcing that produces it. The cumulus mass flux is calculated from profile A and is nonzero in a region extending vertically from $z^* = 0.1$ to the tropopause and radially from $r^* = 0.5$, where the tangential wind goes to zero, outward to $r^* \simeq 13$, where the boundary layer flow becomes divergent, producing descent at the top of the friction layer. The cumuli heat most of the tropospheric column through induction of compensating subsidence in their environment. This process is represented by the first term in the brackets in (16). However, in the upper troposphere, detrainment of cool air from the overshooting cumuli leads to some cooling, and the second term becomes important. The parameterization may underestimate the amount of this second effect because it largely neglects evaporation of detrained condensate. Outside the eye the cloud base mass flux increases toward the center. Thus the buoyancy forcing in this region is negative where the cumuli heat the air and positive where they cool it. Inside the eye the cloud base mass flux decreases to zero, and the signs of the forcing due to heating and cooling are exchanged because of the reversed radial gradient of M_c.

Compensating subsidence also dominates the cumulus momentum forcing in the lower troposphere and the midtroposphere. Because the mean wind decreases with height above the friction layer, the momentum flux is divergent and becomes increasingly so with altitude in this region, but in the upper troposphere, detrainment of high-momentum air makes the flux convergent. The momentum forcing is thus positive below the detrainment layer, negative in the detrainment layer below the level of maximum detrainment, and positive above it. Except in the detrainment layer, where both components are equally important, the momentum forcing is generally about an order of magnitude weaker than the buoyancy forcing.

The secondary circulation induced by this forcing is primarily a positive gyre that extends outward from the eye wall and vertically from the surface to the tropopause. This feature results from the joint action of surface friction and the region of negative forcing due primarily to the horizontal gradient of heating and, to a lesser extent, to the upward increase in momentum convergence below the level of maximum detrainment in the upper troposphere. Within the eye a much weaker negative gyre arises from the reversed horizontal gradient of heating there. Aloft in the outer circulation the inward increase of detrainment cooling forces some descent in the lower stratosphere. This causes the subsidence region of the eye to extend out over the outer vortex, producing a 'stadium effect.' In addition to the detrainment cooling, which may be an artifact of the cumulus parameterization, one would expect cooling due to evaporation of detrained condensate and infrared radiation from the cirrus canopy to contribute to these motions. The predicted descent of stratospheric air into the eye is consistent with *Östland*'s [1968] observation of tritium-rich air from the stratosphere at low levels in the eye of Hurricane Betsy of 1965.

There is no diffusion to import momentum into the eye or to export buoyancy from it. Therefore in this model the gradient of heating is the sole agent capable of maintaining the negative gyre inside the eye. In the case of an intense hurricane that is continuing to intensify, both the cumulus heating and its gradient between the eye wall and the convection-free eye proper should be intense. On the other hand, when the central pressure stops falling in response to weakened heating, the subsidence should also decline. Thus deepening, intense hurricanes should have warm dry eyes, and filling ones should have less subsidence, lower temperatures, and more moisture in their eyes. *Jordan* [1961] has documented this phenomenon with reconnaissance dropsonde data from intense Pacific typhoons.

The generally accepted explanation for the subsidence differs from the foregoing. *Kuo* [1959] and *Malkus* [1958] hypothesize that inward transport of angular momentum from the eye wall causes the wind inside the eye to exceed the gradient value. This leads to outflow at low levels and to subsidence aloft. The angular momentum of the eye wall decreases with height, so the forcing that arises by this mechanism has the appropriate sign to contribute to the subsidence. It is also possible that wave momentum flux convergences may act in a similar fashion. However, the present results indicate that this feature may arise without any horizontal diffusion whatsoever. Furthermore, it is difficult to reconcile Jordan's observations with the diffusion hypothesis because, under that hypothesis, descent should be correlated with intensity itself rather than with the time derivative of intensity.

Other features of these solutions include deep inflow in the outer vortex above the friction layer and a shallow outflow layer confined to the region just below the tropopause. This deep inflow has been observed in nature [e.g., *Frank*, 1977*a*] and is simply the lower half of the large positive gyre. Although the bulk of the mass influx in the model is due to surface friction, the heating gradient in the free atmosphere also contributes to it. The air that converges inward can ascend to the tropopause in the face of the stable stratification only because of the convective heating. At the tropopause the heating ceases, and the air encounters the much greater stability of the lower stratosphere; this restricts its vertical motion and, in combination with upward advection of angular momentum, causes it to turn outward in order to satisfy mass continuity. The radial velocity in the outflow layer is substantially greater than that in the inflow because the density at the tropopause is much less than at the surface. In fact, the outflow velocity is so strong that the validity of the balanced equations is doubtful.

If this calculation is repeated with the cumulus momentum transport suppressed, the strength of the secondary flow and the rate of subsidence in the eye approximately double. Otherwise, the solutions do not differ qualitatively from Figure 5.

Figure 6 shows the effect of elimination of both convective heating and momentum transport. The secondary circulation is forced by surface friction alone. This solution resembles the results of *Estoque* [1962] and *Rosenthal* [1963]. The inflow is confined to the surface friction layer, and the outflow extends through most of the lower and middle troposphere. Perhaps this similarity arises because the heating was either underestimated or excessively concentrated in the lower troposphere in the earlier work.

The secondary circulation in a hurricane over cold water may resemble Figure 6. The air that converges in the friction layer experiences adiabatic cooling and becomes negatively buoyant so that it cannot ascend to the tropopause in the absence of condensational heating. Instead, it satisfies mass continuity by turning outward at relatively low levels. Since the ascent and outflow are confined to the lower troposphere, the upper tropospheric buoyancy anomaly that sustains the low central pressure is largely protected from adiabatic cooling or dissipation by outward advection. This agrees with experience [*Palmen and Newton*, 1969], although many of the long-lived tropical cyclone remnants take on extratropical characteristics.

The final simulation, shown in Figure 7, illustrates the sensitivity of the secondary circulation to the vertical structure of the cumulus mass flux. In this case the forcing is calculated with profile B of Figure 4. The detrainment layer is shallower than with profile A and is not well resolved by the finite

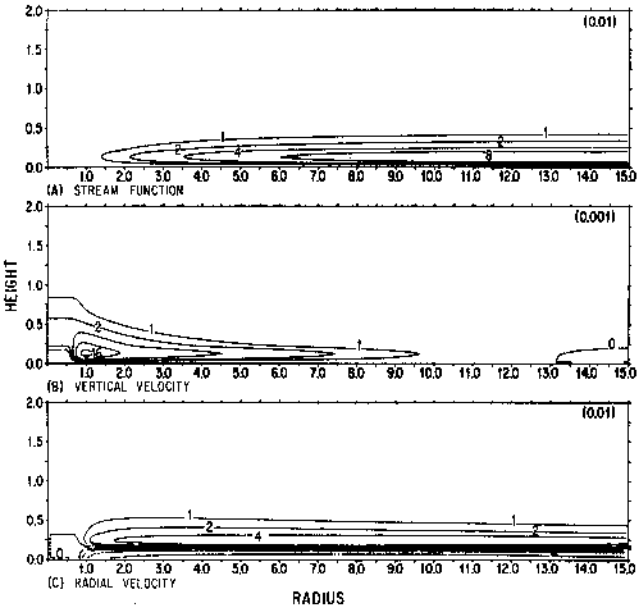

Fig. 6. Frictionally induced secondary circulation with no cumulus processes.

difference grid. Comparison of Figure 5*g* with Figure 7*g* indicates that the region of positive momentum forcing above the level of maximum detrainment is absent because it lies between two information levels. This change in the forcing function leads to profound changes in the secondary circulation. The organized subsidence at high levels inside the eye is replaced by ascent, strong inflow extends nearly to the center in the upper troposphere, and the radial velocity in the outflow layer is greatly increased. The solutions bear little resemblance to hurricanes in nature. Although the eye structure seems to be insensitive to horizontal momentum transports, a spurious convergence of the vertical convective momentum flux is quite another matter. If primitive equation models are equally sensitive to the details of the cumulus fluxes, this may add to the difficulties that have been encountered in implementation of second-generation cumulus parameterizations in hurricane models [*Rosenthal*, 1973, 1979].

CONCLUSIONS

Scale analysis indicates that the balanced equations describe the azimuthally averaged motions in the lower troposphere in hurricanes. This means that the symmetric tangential flow is in gradient and hydrostatic balance and that the radial and vertical motions may be diagnosed if one knows the diabatic processes that act on the flow. However, in the upper tropospheric outflow layer these approximations are weaker because the radial and tangential velocities are comparable. Where the balanced approximation is valid, the asymmetric motions are described by a set of linear equations which indicate that significant departures from gradient balance are possible for point values, as contrasted to the azimuthal mean. Furthermore, the asymmetric motions are not hydrostatic because their aspect ratio is about 1, or alternatively, because the tangential advection frequency approaches the buoyancy frequency.

The solutions obtained for the secondary flow from the balanced equations reveal a number of interesting features. In this model, the subsidence inside the eye arises entirely from the difference in convective heating between the eye wall and the eye itself. It may be that inward diffusion or wave transport

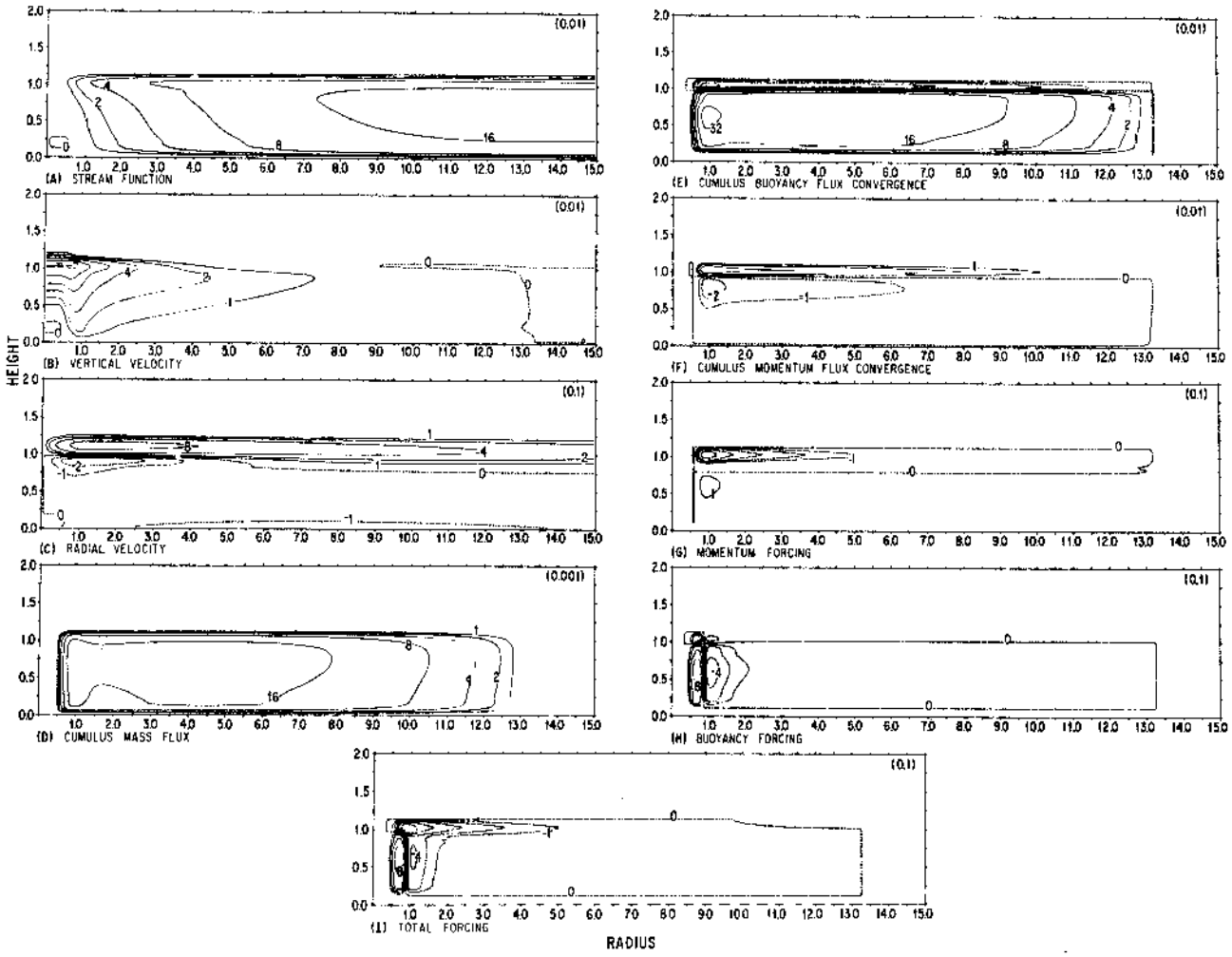

Fig. 7. Secondary circulation and forcing for profile B with momentum transports.

of angular momentum from the eye wall contributes to the forcing of the subsidence in nature, but the descent in the eye is observed to be correlated with the rate of change of intensity rather than with intensity itself. These observations seem to be inconsistent with the view that momentum diffusion is primarily responsible for the subsidence. The deep inflow present in the outer vortex is caused by the inward increase in convective heating. The heating also enables the air to ascend to the tropopause, where it turns outward after encountering the greater stability of the stratosphere. If the heating were not present, the outflow would occur in a shallow layer confined to the lower troposphere, and the buoyancy anomaly would be somewhat protected from any influx of cold air in the boundary layer.

The secondary flow is sensitive to the vertical structure of the cumulus mass flux. If its structure is adequately resolved, cumulus momentum transports tend to weaken somewhat the secondary circulation and, in conjuction with cold detrainment, to induce subsidence in the lower stratosphere. On the other hand, if the detrainment layer is not resolved in enough detail, the momentum transports may lead to rising motion that extends completely across the eye. In hurricane simulations it is perhaps better to ignore cumulus momentum effects than to model them badly.

Acknowledgments. This paper has been substantially improved as a result of discussions with L. N. Lahiff, R. E. Lopez, and S. L. Rosenthal. Dave Jorgensen made the Anita aircraft data available, and both he and Steve Datzman assisted greatly in processing it. I am also grateful to Thom Maloney and Dale Martin for their skillful help with the manuscript and illustrations.

REFERENCES

Anthes, R. A., A numerical model of the slowly varying tropical cyclone in isentropic coordinates, *Mon. Weather Rev., 99*, 617–635, 1971.

Anthes, R. A., The dynamics and energetics of mature tropical cyclones, *Rev. Geophys. Space Phys., 12*, 495–522, 1974.

Anthes, R. A., S. L. Rosenthal, and J. Trout, Preliminary results from an asymmetric model of the tropical cyclone, *Mon. Weather Rev., 99*, 744–758, 1971.

Arakawa, A., and W. Schubert, Interaction of a cumulus cloud ensemble with the large scale environment, I, *J. Atmos. Sci., 31*, 674–701, 1974.

Charney, J. C., and A. Eliassen, On the growth of the hurricane depression, *J. Atmos. Sci., 21*, 68–75, 1964.

Eliassen, A., Slow thermally or frictionally controlled meridional circulation in a circular vortex, *Astrophys. Norv., 5*, 19–60, 1951.

Estoque, M. A., Vertical and radial motions in a tropical cyclone, *Tellus, 14*, 395–402, 1962.

Fraedrich, K., On the parameterization of cumulus convection by lateral mixing and compensating subsidence, I, *J. Atmos. Sci., 30*, 408–413, 1973.

Frank, W. M., The structure and energetics of the tropical cyclone, I, Storm structure, *Mon. Weather Rev., 105,* 1119–1135, 1977*a*.

Frank, W. M., Convective fluxes in tropical cyclones, *J. Atmos. Sci., 34,* 1554–1568, 1977*b*.

Gray, W. M., and D. J. Shea, The hurricane's inner core region, II, Thermal stability and dynamic characteristics, *J. Atmos. Sci., 30,* 1565–1576, 1973.

Hawkins, H. F., and D. T. Rubsam, Hurricane Hilda, 1964, II, Structure and budgets of the hurricane on October 1, 1964, *Mon. Weather Rev., 96,* 617–636, 1968.

Hayes, F. R., A new parameterization of deep convection for use in a 10-level model, *Quart. J. Roy. Meteorol. Soc., 103,* 359–367, 1977.

Holton, J. R., *Introduction to Dynamic Meteorology,* pp. 228–234, Academic, New York, 1972.

Holton, J. R., *The Dynamic Meteorology of the Stratosphere and Mesophere,* American Meteorological Society, Boston, Mass., 1975.

Johnson, R. H., The role of convective-scale precipitation downdrafts in cumulus and synoptic-scale interaction, *J. Atmos. Sci., 33,* 1890–1910, 1976.

Jones, R. W., A nested grid for a three-dimensional model of a tropical cyclone, *J. Atmos. Sci., 34,* 1528–1553, 1977.

Jordan, C. L., Marked changes in the characteristics of the eye of intense typhoons between the deepening and filling stages, *J. Meteorol., 18,* 779–789, 1961.

Kuo, H. L., Dynamics of convective vortices and eye formation, in *The Atmosphere and the Sea in Motion,* edited by B. Bolin, pp. 413–424, Rockefeller Institute Press, New York, 1959.

Kuo, H. L., On the formation and intensification of tropical cyclones through latent heat release by cumulus convection, *J. Atmos. Sci., 22,* 40–63, 1965.

Kurihara, Y., and R. E. Tuleya, Structure of a tropical cyclone developed in a three-dimensional numerical simulation model, *J. Atmos. Sci., 31,* 893–919, 1974.

Lindzen, R. S., and H. L. Kuo, A reliable method for the numerical integration of a large class of ordinary and partial differential equations, *Mon. Weather Rev., 97,* 732–734, 1969.

Malkus, J. S., On the structure and maintenance of the mature hurricane eye, *J. Meteorol., 15,* 337–349, 1958.

Mathur, M. B., A multiple-grid, primitive equation model to simulate the development of an asymmetric hurricane (Isbell, 1964), *J. Atmos. Sci., 31,* 371–393, 1974.

Ogura, Y., Frictionally controlled, thermally driven circulation in a circular vortex with applications to tropical cyclones, *J. Atmos. Sci., 21,* 610–621, 1964.

Ogura, Y., and H. Cho, Diagnostic determination of cumulus cloud populations from large-scale variables, *J. Atmos. Sci., 30,* 1276–1286, 1973.

Ogura, Y., and N. A. Phillips, Scale analysis of deep and shallow convection in the atmosphere, *J. Atmos. Sci., 19,* 173–179, 1962.

Ooyama, K., Numerical simulation of the life-cycle of tropical cyclones, *J. Atmos. Sci., 26,* 3–40, 1969.

Ooyama, K., Theory on parameterization of cumulus convection, *J. Meteorol. Soc. Jap., 49,* 744–756, 1971.

Östland, H. G., Hurricane tritium II: Air-sea exchange of water in Betsy 1965, *Tellus, 20,* 577–594, 1968.

Palmen, E., and C. W. Newton, *Atmospheric Circulation Systems,* pp. 515–519, Academic, New York, 1969.

Peng, L., and H. L. Kuo, A numerical simulation of the development of tropical cyclones, *Tellus, 27,* 133–144, 1975.

Rosenthal, S. L., On the problem of the diagnostic calculation of vertical and radial motions in a wet vortex, *Mon. Weather Rev., 91,* 453–464, 1963.

Rosenthal, S. L., Experiments with a numerical model of tropical cyclone development: Some effects of radial resolution, *Mon. Weather Rev., 98,* 106–120, 1970*a*.

Rosenthal, S. L., A circularly symmetric primitive equation model of tropical cyclone development containing an explicit water vapor cycle, *Mon. Weather Rev., 98,* 643–663, 1970*b*.

Rosenthal, S. L., Hurricane modeling experiments with a new parameterization for cumulus convection, *NOAA Tech. Memo. ERL WMPO-4,* Nat. Oceanic and Atmos. Admin., Boulder, Colo., 1973.

Rosenthal, S. L., Numerical simulation of tropical cyclone development with latent heat release by resolvable scales, I, Model description and preliminary results, *J. Atmos. Sci., 35,* 258–271, 1978.

Rosenthal, S. L., The sensitivity of simulated hurricane development to cumulus parameterization details, *Mon. Weather Rev., 107,* 193–197, 1979.

Schneider, E. K., and R. S. Lindzen, A discussion of the parameterization of momentum exchange by cumulus convection, *J. Geophys. Res., 81,* 3158–3160, 1976.

Shea, D. J., and W. M. Gray, The hurricane's inner core region, I, Symmetric and asymmetric structure, *J. Atmos. Sci., 30,* 1544–1564, 1973.

Sheets, R. C., On the evolution of Hurricane Anita (1977), in *11th Technical Conference on Hurricanes and Tropical Meteorology,* pp. 459–465, American Meteorological Society, Boston, Mass., 1977.

Sundqvist, H., Numerical simulation of the development of tropical cyclones with a ten-level model, I, *Tellus, 22,* 359–390, 1970*a*.

Sundqvist, H., Numerical simulation of the development of tropical cyclones with a ten-level model, II, *Tellus, 22,* 504–510, 1970*b*.

Willoughby, H. E., Inertia-buoyancy waves in hurricanes, *J. Atmos. Sci., 34,* 1028–1039, 1977.

Willoughby, H. E., A possible mechanism for the formation of hurricane rainbands, *J. Atmos. Sci., 35,* 838–848, 1978*a*.

Willoughby, H. E., The vertical structure of hurricane rainbands and their interaction with the mean vortex, *J. Atmos. Sci., 35,* 849–858, 1978*b*.

Yamasaki, M., A tropical cyclone model with parameterized vertical partition of released latent heat, *J. Meteorol. Soc. Jap., 46,* 202–214, 1968*a*.

Yamasaki, M., Detailed analysis of a tropical cyclone simulated with a 13-layer model, *Pap. Meteorol. Geophys., 19,* 559–585, 1968*b*.

Yamasaki, M., A preliminary experiment of the tropical cyclone without parameterizing the effects of cumulus convection, *J. Meteorol. Soc. Jap., 55,* 11–30, 1977*a*.

Yamasaki, M., The role of surface friction in tropical cyclones, *J. Meteorol. Soc. Jap., 55,* 559–571, 1977*b*.

Yanai, M., S. Esbensen, and J. Chu, Determination of bulk properties of tropical cloud clusters from large-scale heat and moisture budgets, *J. Atmos. Sci., 30,* 611–627, 1973.

(Received June 29, 1978;
revised January 8, 1979;
accepted January 11, 1979.)